Sensitivity of Thin Cirrus Clouds in the Tropical Tropopause Layer to Ice Crystal Shape and Radiative Absorption

R. D. Russotto,[1] T. P. Ackerman,[1,2] D. R. Durran[1]

[1]Department of Atmospheric Sciences, University of Washington, Seattle, WA, USA.

[2]Joint Institute for the Study of the Atmosphere and Ocean, University of Washington, Seattle, WA, USA.

This article has been accepted for publication and undergone full peer review but has not been through the copyediting, typesetting, pagination and proofreading process, which may lead to differences between this version and the Version of Record. Please cite this article as doi: 10.1002/2015JD024413

Abstract. Subvisible cirrus clouds in the tropical tropopause layer (TTL) play potentially important roles in Earth's radiation budget and in the transport of water into the stratosphere. Previous work on these clouds with 2D cloud-resolving models has assumed that all ice crystals were spherical, producing too few crystals greater than 60 microns in length compared with observations. In this study, the System for Atmospheric Modeling (SAM) cloud-resolving model is modified in order to calculate the fall speeds, growth rates, and radiative absorption of non-spherical ice crystals. This extended model is used in simulations that aim to provide an upper bound on the effects of ice crystal shape on the time evolution of thin cirrus clouds and to identify the physical processes responsible for any such effects. Model runs assuming spheroidal crystals result in a higher center of cloud ice mass than in the control, spherical case, while the total mass of ice is little affected by the shape. Increasing the radiative heating results in less total cloud ice mass relative to the control case, an effect which is robust with more extreme perturbations to the absorption coefficients. This is due to higher temperatures reducing the relative humidity in the cloud and its environment, and greater entrainment of dry air due to dynamical changes. Comparisons of modeled ice crystal size distributions with recent airborne observations of TTL cirrus show that incorporating non-spherical shape has the potential to bring the model closer to observations.

Keypoints:

- We extended a model of optically thin TTL cirrus to include non-spherical ice crystal shapes.

- Shape has little impact on cloud dynamics due to competing effects and small ice crystal size.

- Increasing the radiative heating lofts the cloud higher but reduces its total mass.

1. Introduction

Optically thin cirrus clouds in the tropical tropopause layer (TTL), a layer with properties of both the troposphere and stratosphere between about 14.0 and 18.5 km altitude [*Fueglistaler et al.*, 2009], are a topic of interest in the atmospheric science community because of their potential impacts on Earth's radiation budget and on stratospheric water vapor. Satellite [e.g. *Wang et al.*, 1996; *Mace et al.*, 2009; *Virts and Wallace*, 2010] and ground-based [*Comstock et al.*, 2002] observations have shown that thin cirrus are common in the TTL. A subset of these clouds, known as "subvisible" cirrus, have very small shortwave optical depths (the precise definition varies, but one reasonable definition is $\tau < 0.02$ in the shortwave, following *Dinh et al.* [2012]). While the direct radiative impact of clouds that thin on the surface is very small [*Lee et al.*, 2009], subvisible TTL cirrus have the potential to affect climate indirectly by regulating the transport of water vapor into the stratosphere [*Jensen et al.*, 1996; *Corti et al.*, 2006; *Dinh et al.*, 2012, 2014; *Dinh and Fueglistaler*, 2014a, b].

Due to the impacts of stratospheric water vapor on surface climate [*Solomon et al.*, 2010], a good physical understanding of the role TTL cirrus play in its regulation is important for predictions of future climate. Stratospheric water vapor is also of interest for playing key roles in catalyzing stratospheric ozone depletion, both in gas phase [*Dvortsov and Solomon*, 2001] and mixed phase [*Solomon et al.*, 1986] chemistry.

The complexity of the interactions between TTL cirrus and troposphere-stratosphere water vapor exchange, as well as a more general desire to understand how these clouds are formed and maintained, has motivated modeling studies of these clouds. These studies

have included 1-D models following Lagrangian parcel trajectories [e.g. *Jensen and Pfister*, 2004; *Jensen et al.*, 2008; *Ueyama et al.*, 2014], 2-D cloud-resolving model simulations [*Durran et al.*, 2009; *Dinh et al.*, 2010; *Dinh and Durran*, 2012; *Dinh et al.*, 2012, 2014; *Dinh and Fueglistaler*, 2014a], larger-scale 2-D simulations in which clouds are idealized as heat sources [*Dinh and Fueglistaler*, 2014b], and 3-D cloud-resolving model simulations [*Jensen et al.*, 2011; *Podglajen et al.*, 2015].

Our study builds on the 2-D model studies cited above, particularly those by *Durran et al.* [2009], *Dinh et al.* [2010] and *Dinh et al.* [2012], so we discuss these studies in more detail here. *Durran et al.* [2009] and *Dinh et al.* [2010] began with an existing cloud in the absence of any large scale motion, and studied the dynamical response of the cloud to the radiative heating of the ice crystals. *Dinh et al.* [2010] used a model that explicitly calculated diffusional growth rates and fall speeds for spherical ice crystals of various radii, and showed that radiative heating of the cloud ice induced a circulation that maintained the cloud against diabatic heating and sedimentation. This provided a mechanism to explain observations of TTL cirrus persisting for several days [*Winker and Trepte*, 1998; *Taylor et al.*, 2011]. *Dinh et al.* [2012] simulated thin TTL cirrus nucleated from a moist patch due to a passing Kelvin wave, in order to demonstrate that these clouds could be maintained against sedimentation by the radiatively induced circulation in the presence of large-scale motions and to investigate the effects of these clouds on the redistribution of water vapor in the TTL.

The importance of the circulation induced by radiative heating of ice crystals in sub-visible TTL cirrus suggests that we should pay careful attention to the realism of the microphysics and radiative transfer schemes used in these studies. The 2-D dynamical

model simulations mentioned above have assumed that all ice crystals are spherical, which results in discrepancies between modeled and observed ice crystal size distributions, particularly for larger crystals. More specifically, *Dinh et al.* [2012] found that the assumption of spherical crystals led to an underestimate of the concentrations of crystals > 20 μm in length, compared with observations. It was hypothesized that explicitly including non-spherical ice crystals in the model's microphysics and radiative transfer schemes would help improve the model's agreement with observations, because non-spherical particles fall more slowly than spheres of the same mass and would therefore be expected to remain in the cloud, where they would grow, for a longer time before falling out.

Previous modeling work considering non-spherical ice crystals in subvisible TTL cirrus is limited. *Jensen et al.* [2008] considered hexagonal plate crystals in TTL cirrus, but this was in a 1-D, trajectory-following model, not a 2-D model as considered here. Other cloud resolving modeling modeling studies have considered non-spherical ice crystals, but not in the specific context of subvisible TTL cirrus. For example, the *Avramov and Harrington* [2010] study of mixed-phase Arctic clouds involved a very detailed microphyiscs scheme involving 7 hydrometeor species, and case studies of mid-latitude cirrus have included non-spherical crystals in their detailed microphysics schemes [*Wu et al.*, 2000; *Cheng et al.*, 2001; *Sölch and Kärcher*, 2011].

The objective of this study is to investigate whether the spherical shape assumption presents a significant source of error in the modeling of subvisible TTL cirrus properties, and to identify the specific physical processes responsible for any effects that ice crystal shape has on the cloud evolution. To determine an upper bound on the possible effects of ice crystal shape on the evolution and maintenance of thin TTL cirrus, we have in-

corporated non-spherical ice crystals into the System for Atmospheric Modeling (SAM) cloud-resolving model using relatively simple, approximate methods, for ice crytals with a conservatively large aspect ratio. We analyze the sensitivity of the cloud evolution to changes in the ice crystal shape using cloud-resolving model experiments similar to those performed by *Dinh et al.* [2010]. We change the fall speed, growth rate and radiative absorption calculations one at a time in order to determine which physical processes are responsible for the simulated effects of shape. Also, we run some additional sensitivity tests to more extreme perturbations in the physics, particularly the radiative heating, in order to gain a better physical understanding of the dynamics of thin TTL cirrus.

2. Model description

The cloud-resolving model used here is based on the System for Atmospheric Modeling (SAM), described in *Khairoutdinov and Randall* [2003]. *Dinh et al.* [2012] replaced the SAM advection scheme with the selective monotonicity-preserving scheme described by *Blossey and Durran* [2008]. We have used the same dynamical core as *Dinh et al.* [2012].

The model domain is 2-dimensional. The location is assumed to be on the equator, so that the Coriolis force can be ignored. The vertical resolution is 25 m and the horizontal resolution is 100 m, the same as in *Dinh et al.* [2010] but finer than *Dinh et al.* [2012]. The domain extends 432 km in the x-direction and 3.25 km in the z-direction, from 14.75 km to 18 km.

The initial ice crystal number concentration field is the same as that in *Dinh et al.* [2010], with a maximum concentration of 1.3×10^{-6} m^{-3} in the center of the cloud. The ice crystal size distribution is initially monodisperse, with ice crystals of radius 3.0 μm, or in the case of non-spherical crystals, having the equivalent mass of a 3-micron-radius

sphere. Nucleation of new ice crystals is not considered, but ice crystals can grow or shrink by deposition or sublimation, respectively. The initial temperature and humidity profiles are the same as those used in *Dinh et al.* [2010] and are shown in Figure 1. The temperature profile used is statically stable throughout the domain (Figure 1b). The initial water vapor profile is set so that the relative humidity with respect to ice (RH_i) is 100% in the cloud layer, including to the sides of the cloud extending out to the edges of the domain, and 80% above and below the cloud layer.

For the dynamics, periodic boundary conditions are used on the lateral edges and the non-reflective, open boundary conditions described by *Bougeault* [1983] and *Klemp and Durran* [1983] are used at the top and bottom of the domain. The radiative fluxes impinging on the cloud are precalculated using a radiative transfer model for a clear-sky case in a typical tropical atmosphere. The radiative fluxes exiting the cloud layer are calculated using the scheme described in Section 4.

3. Microphysics scheme

3.1. Spherical case

We use the bin microphysics scheme of *Dinh and Durran* [2012], which contains 25 size bins and employs a cubic size distribution function within each bin. One new aspect of our simulations is that the fall speeds of ice crystals are calculated according to Stokes flow theory rather than the *Böhm* [1989] formula used by *Durran et al.* [2009] and *Dinh et al.* [2010, 2012]. This is done for theoretical consistency with the spheroid corrections described in Section 3.2. The terminal velocity in the Stokes flow regime is found according

to [*Lamb and Verlinde*, 2011, p. 388]:

$$v = \frac{2}{9}\frac{\rho_{\text{ice}} g}{\mu_{\text{air}}} r^2 \tag{1}$$

where ρ_{ice} is the density of ice, g is the acceleration due to gravity, μ_{air} is the dynamic viscosity of air, and r is the radius of the spherical ice crystal. This expression is valid when the particle is much larger than the mean free path of air and the Reynolds number is much less than 1 [*Lamb and Verlinde*, 2011, p. 386], which is a reasonable assumption for the small ice crystals found in thin TTL cirrus.

As in *Dinh et al.* [2010], the rate of growth of spherical ice crystals by deposition is calculated according to [*Pruppacher and Klett*, 1978, equation 13-71]:

$$\frac{\mathrm{d}m}{\mathrm{d}t} = \frac{4\pi C \left(S_{\text{ice}} - 1\right)}{\frac{R_v T}{e_{\text{sat,ice}} D'_v} + \frac{L_s}{k'_a T}\left(\frac{L_s}{R_v T} - 1\right)} \tag{2}$$

where m is the mass of the ice crystal, C is the capacitance (equal to the radius for a sphere), $e_{\text{sat,ice}}$ is the saturation vapor pressure over a planar ice surface, S_{ice} is the saturation ratio with respect to ice, R_v is the gas constant for water vapor, T is the temperature in Kelvin, D'_v is the modified diffusivity of water vapor in air, k'_a is the modified thermal conductivity of air, and L_s is the latent heat of sublimation of ice. This calculation does not take into account the direct impact of radiative heating on ice crystal growth, but such effects are negligible for ice crystals smaller than a few tens of microns in length [*Gierens*, 1994] and are therefore irrelevant to our study.

3.2. Non-spherical case

The ice crystal shapes that we are most interested in representing are hexagonal plates and columns, because these are the most common regularly shaped crystals observed in subvisible TTL cirrus, although other shapes such as triangles and irregular crystals are

also present [*Lawson et al.*, 2008]. Simulation of the microphysical properties of plates and columns is difficult due to the lack of analytical solutions. Because of this, we have chosen to represent plates and columns using oblate and prolate spheroids, respectively, following *Jensen et al.* [2008]. We use oblate and prolate spheroids with aspect ratios of 6:1.

We obtained this value from Appendix A of *Lawson et al.* [2008], who computed the aspect ratio of a hexagonal ice crystal photographed in subvisible TTL cirrus during the Costa Rica Aura Validation Experiment (CR-AVE) using the Cloud Particle Imager (CPI) instrument. The aspect ratios of many imaged particles could not be determined either because the particles were too small or because they were not aligned so that all the necessary features could be seen, but the example given indicates that this is a reasonable aspect ratio for ice crystals larger than 65 microns in diameter. For ice crystals smaller than 65 microns, which account for most of the particles in our model, the habit and aspect ratio of the ice crystals cannot be determined from CPI images because the image resolution is too low, but such small crystals do appear to be fairly close to equidimensional. Therefore, our assumption of a fixed aspect ratio of 6 for all ice crystals likely means the small crystals in our model are more elongated than their real-world counterparts of the same mass, and our experiments provide an upper bound on the effects of shape rather than a best estimate. As we will see, the effect of ice crystal shape on our simulated cloud evolution even in this extreme case is fairly small, so if the ice crystals were closer to spheres, the effect would be even smaller and our conclusion that ice crystal shape did not significantly affect the dynamics of subvisible TTL cirrus would be unchanged. Also, it has been pointed out [*Ulanowski et al.*, 2004] that a rosette-like

structure on the order of 50 microns across could appear roughly spherical when viewed by the CPI. The non-sphericity of such a particle would affect its radiative properties [*Um and McFarquhar*, 2011], as well as, presumably, its fall speed and diffusional growth rate, because its surface area to volume ratio would be greater than that for a sphere, as in the case of an elongated spheroid.

3.2.1. Fall Speed

For the terminal fall speeds of the spheroidal ice crystals, we use corrections to the spherical fall speeds that are functions only of the aspect ratio and independent of the ice crystal size. These corrections are given by *Fuchs* [1964, pp. 37-40] and are based on Stokes flow theory. The preferred orientations of falling ice crystals are those which present the largest possible horizontal cross-sectional area. For oblate spheroids, this means that the polar axis (the axis of revolution) is oriented vertically; for prolate spheroids, the polar axis is oriented horizontally. For an oblate spheroid falling along the polar axis, the correction is

$$\kappa = \frac{\frac{4}{3}\left(\beta^{1/3}\right)\left(\beta^2-1\right)}{\frac{\beta(\beta^2-2)}{\sqrt{\beta^2-1}}\tan^{-1}\left(\sqrt{\beta^2-1}\right)+\beta} \tag{3}$$

where κ is the ratio of the spherical to the spheroidal particle's fall speed, also known as the "dynamic shape factor", and β is the spheroid's aspect ratio, or the ratio of its major to minor axis. For a prolate spheroid falling transverse to the polar axis, the dynamic shape factor is

$$\kappa = \frac{\frac{8}{3}\left(\beta^{-1/3}\right)\left(\beta^2-1\right)}{\frac{(2\beta^2-3)}{\sqrt{\beta^2-1}}\ln\left(\beta+\sqrt{\beta^2-1}\right)+\beta}. \tag{4}$$

Figure 2 shows the inverse dynamic shape factor, $1/\kappa$, for oblate and prolate spheroids of various aspect ratios calculated using Equations 3 and 4, respectively. This is the factor by which the ice crystals' fall speeds are reduced by the non-spherical shape if their mass

is held constant. For an aspect ratio of 6, used in the model simulations, fall speeds are reduced by about 1/3.

3.2.2. Growth Rate

To calculate the growth rates of spheroids, different expressions for capacitance are used in Equation 2. For an oblate spheroid, the capacitance is [*Pruppacher and Klett*, 1978, Eq. 13-73]:

$$C_{\text{oblate}} = \frac{ae}{\sin^{-1} e} \tag{5}$$

where a is the semi-major axis of the ellipse of revolution and e is the ellipse's eccentricity, defined as

$$e = \sqrt{1 - \frac{b^2}{a^2}} \tag{6}$$

where b is the semi-minor axis of the ellipse of revolution. For a prolate spheroid, the capacitance is [*Pruppacher and Klett*, 1978, Eq. 13-74]:

$$C_{\text{prolate}} = \frac{A}{\ln\left(\frac{a+A}{b}\right)} \tag{7}$$

where A is the linear eccentricity, defined as

$$A = \sqrt{a^2 - b^2}. \tag{8}$$

Note that the calculations of D'_v and k'_a in Equation 2 depend on the radius in the spherical case, and it is not completely obvious whether capacitance should replace radius in those calculations as well. In this case we have used capacitance, but the calculated growth rate is very sensitive to other possible choices such as the semi-major or semi-minor axis. See Section S1 in the Supplemental Information for more details on the growth rate calculation and this potential source of uncertainty.

Another source of uncertainty in the growth rate is the choice of the deposition coefficient of ice. We have assumed a constant value of 0.01 for this coefficient. This is a fairly commonly used value within an order of magnitude of the value of 0.006 determined by the laboratory experiments of *Magee et al.* [2006]. *Zhang and Harrington* [2015] argue that a value close to 1 for the deposition coefficient is more appropriate when homogeneous freezing is being considered but is less appropriate after ice crystals are already nucleated, which is assumed from the start in our simulations. The parcel model simulations of *Zhang and Harrington* [2015] predict values of the deposition coefficient ranging from 0.001 to 1 depending on environmental factors and ice crystal shape. *Dinh* [2012] explored the sensitivity of simulated TTL cirrus to the deposition coefficient in the SAM model and found that the choice of deposition coefficient significantly affects the cloud evolution.

To understand the effects of the non-spherical shape on the growth of an individual ice crystal, Figure 3 shows the ratio of the mass growth rate for an oblate or prolate spheroidal ice crystal to that for a sphere of the same mass. The growth rate depends on the temperature and pressure, so the plot assumes a temperature of 190 K and a pressure of 135 hPa, typical values for the TTL. Unlike for the fall speed, the growth rate depends on the mass in addition to the aspect ratio, so the plot assumes an aspect ratio of 6 (used in the sensitivity tests in Section 5.1) and shows results for the range of masses considered in bin microphysics scheme. The mass is expressed in terms of the radius of the equivalent-mass sphere. Figure 3 shows that assuming a spheroidal shape with an aspect ratio of 6 increases the magnitude of $\mathrm{d}m/\mathrm{d}t$ by a factor of between about 1.4 and 1.7, depending on the mass and whether the spheroid is oblate or prolate. Note, however,

that this does not necessarily mean that spheroidal ice crystals will grow to larger sizes; if they are in a subsaturated environment, they will sublimate faster than their spherical counterparts.

4. Radiation scheme

4.1. Spherical case

Following the method first outlined in *Durran et al.* [2009, Section 3a], we calculate the radiative heating in each cloudy model layer based on the convergence of broadband longwave (LW) and shortwave (SW) fluxes at the top and bottom of that layer using a simplified, 1D, plane-parallel radiative transfer solver. The cloud absorption is calculated using broadband LW and SW absorption coefficients that are parameterized for different ice crystal masses spanning the microphysics size bins. The absorption coefficients are tuned so that the radiative heating rate produced by the cloud-resolving model's radiative transfer scheme matches that produced by a spectrally resolved radiative transfer model run for a typical subvisible TTL cirrus cloud. *Durran et al.* [2009] performed this parameterization for spherical crystals. We have redone the parameterization for the LW coefficients for non-spherical crystals. Some details of the parameterization process have not been discussed in previous papers but are important to the effects of shape on the radiative absorption, so we describe the process in greater detail here.

The basic steps of the parameterization process are enumerated below, and then discussed in more detail:

1. For a particular ice crystal radius, calculate the single-scattering properties (extinction cross section, absorption cross section, and asymmetry factor) of the ice crystals as a function of wavelength using a Mie scattering code.

2. Feed these single-scattering properties into a 1D, spectrally resolved, multiple-scattering radiative transfer model for a cloud layer typical of subvisible TTL cirrus and calculate the radiative fluxes entering and leaving the cloud.

3. Invert the radiative transfer solver used in the cloud-resolving model in order to find a broadband absorption cross section such that the cloud-resolving model produces approximately the same radiative heating rate as the radiative transfer model for the same cloud layer.

For Step 1, we used the values of the real and imaginary indices of refraction of ice compiled by *Warren and Brandt* [2008]. For the Mie scattering calculation, *Durran et al.* [2009] used the code written by *Toon and Ackerman* [1981]. We instead used the T-Matrix code [*Mishchenko and Travis*, 1998] for the Mie scattering calculation, so that we would have a more general method that would work for either spheres or spheroids. We verified that the two codes produced virtually identical output when given identical inputs in the spherical case.

For Step 2, we used the standalone version of the Rapid Radiative Transfer Model (RRTM). In RRTM, the absorption calculation is based on *Mlawer et al.* [1997], except that two of the band boundaries are changed. Scattering is calculated using the discrete-ordinates method [DISORT; *Stamnes et al.*, 1988, 2000]. RRTM can be run with the 4, 8, or 16-stream version of DISORT; the 4-stream version is sufficient for our purposes because we are only interested in the overall longwave heating of the cloud layer, for which scattering is relatively unimportant. We ran RRTM for a cloud layer between 16.0 and 16.5 km altitude and having an optical thickness of 0.005, with the temperature and

humidity profiles taken from a March climatological average in the Galápagos [*Gettelman et al.*, 2004].

Step 3 of the parameterization involves a simple analytical expression which can be derived from the radiative transfer scheme in SAM. The broadband absorption cross section σ_a can be found using:

$$\sigma_a = \frac{-\ln\left(1 - \frac{FC_{\text{ice}}}{F^{\uparrow}_{\text{bot}} + F^{\downarrow}_{\text{top}} - 2B}\right)}{2N\Delta z} \tag{9}$$

where FC_{ice} is the radiative flux convergence in the cloud layer calculated in Step 2 minus the radiative flux convergence in the same layer in a clear-sky case; $F^{\uparrow}_{\text{bot}}$ and $F^{\downarrow}_{\text{top}}$ are the radiative fluxes impinging on the cloud layer; B is the blackbody emission of the cloud layer (based on the average temperature of the cloud layer in the RRTM input sounding); N is the number concentration of ice crystals; and Δz is the thickness of the cloud layer.

The longwave and shortwave absorption cross sections for spherical crystals obtained using these methods are shown in Table 1. The SW version is the same as that originally calculated by *Durran et al.* [2009], with a subsequent extension to larger ice crystal sizes. The LW version is similar to the original, but with minor changes associated with the methodological changes we have adopted (a different radiative transfer model and updated optical constants of ice). We use these revised values for methodological consistency with the non-spherical adjustment described in Section 4.2.

We have not redone the radiation parameterization in the shortwave because shortwave absorption is relatively unimportant for the small ice crystal sizes and optical depths considered. Comparing the Zero SW Absorption case to the Control case in Figure 7 shows that shutting off the SW absorption makes very little difference to the cloud evolution.

Therefore, small changes to the shortwave absorption due to shape effects would have negligible effects on the cloud.

4.2. Non-spherical case

Incorporating the radiative properties of non-spherical ice crystals into the model requires redoing Step 1 of the parameterization of absorption cross sections described in Section 4, namely the calculation of the single scattering properties and phase function moments of the ice crystals. For non-spherical crystals, there is no method for calculating single-scattering properties and phase functions of ice crystals that is both exact and computationally cheap across the full range of ice crystal sizes in our microphysics scheme. We had intended to use the T-Matrix code to calculate the single-scattering properties of spheroids directly, but this code fails to converge at large size parameters, and this limit is reached within the size range considered in our model for aspect ratios of 6. Previously, a method was developed to calculate the single-scattering properties of individual [*Asano and Yamamoto*, 1975] or randomly oriented [*Asano and Sato*, 1980] oblate or prolate spheroids of arbitrary aspect ratio. This method should, in theory, work for all size parameters, but we have not been able to create a working code. Several databases [*Fu et al.*, 1998; *Yang et al.*, 2013] of the single-scattering properties of hexagonal plates and columns have been compiled based on extensive calculations, but these databases assume an aspect ratio that changes as a function of ice crystal mass, and they are nearly equidimensional for the masses considered in our model. *Yang et al.* [2013] have performed calculations for spheroids with fixed aspect ratios, but not for an aspect ratio of 6. Performing new calculations in the manner of *Yang et al.* [2013] is very time-consuming because an empirical correction process is required to reconcile differences between the

Improved Geometric Optics Method [*Bi et al.*, 2009] and Mie scattering results for the sizes where the two methods overlap, and this correction needs to be done for each of the 16 RRTM bands for each shape.

Therefore, we adopted a simplified approximation of columns and plates for the radiation parameterization. This method involves representing a cloud of randomly oriented, non-spherical ice crystals using spheres with the same surface area to volume ratio (referred to as "equal-V/A spheres" hereafter), with the number concentration adjusted to conserve mass. The accuracy of this method for the calculation of upward and downward fluxes of radiation in multiple-scattering radiative transfer models was first demonstrated by *Grenfell and Warren* [1999], who considered the case of cylindrical ice crystals. *Neshyba et al.* [2003] extended this method to solid, hexagonal plates and columns, and *Grenfell et al.* [2005] further extended it to hollow columns and plates. The rationale for this method is that the scattering caused by a cloud layer depends mainly on the total ice crystal surface area and the absorption depends mainly on the total volume of ice, while the number concentration of ice crystals is not very important for the radiative fluxes if total mass is held constant.

We used the equal-V/A spheres method for hexagonal columns and plates, following *Neshyba et al.* [2003]. After calculating the single-scattering properties of the equal-V/A spheres (we used the T-Matrix code for this although the *Toon and Ackerman* [1981] code would also have worked), we ran RRTM with the number concentration of equal-V/A spheres set so that the cloud ice volume was the same as in the original parameterization (but the number of particles and the total surface area were greater). After running RRTM, we found the absorption cross section for the column or plate using Equation 9;

the value of N substituted into Equation 9 was the number of non-spherical particles, not the number of equal-V/A spheres.

The parameterized absorption cross sections for spheres, plates and columns in the longwave, and for spheres in the shortwave, are shown in Table 1. Based on several other methods tried for doing this parameterization for non-spherical crystals, we estimate the error in the plate and column absorption cross sections to be about $\pm$ 15% (see Section S2 in the Supplemental Information for how we arrived at this estimate). Figure 4 shows the ratios of the parameterized longwave absorption cross sections for plates and columns to those for spheres. For larger ($>$ 10 μm in equivalent-mass sphere radius) crystals, the non-spherical crystals absorb 50-60% more LW radiation than their spherical counterparts. For smaller crystals, the effect diminishes until the absorption coefficients are about the same for the very smallest crystals considered. Our SAM simulations assume an initial equivalent-mass sphere radius of 3.0 μm, for which the columns and plates absorb only about 10% more radiation than the spheres.

5. Model sensitivity tests

We ran a control SAM simulation analogous to the control case in *Dinh et al.* [2010], and sensitivity tests to changes in the physical assumptions for the model's fall speed, growth rate and radiative absorption calculations. Section 5.1 discusses tests of the sensitivity of the cloud evolution to ice crystal shape using the corrections described in Sections 3.2 and 4.2, while Section 5.2 describes the results of tests of the sensitivity to more extreme physical assumptions intended to better understand the physical reasons for the results of the shape tests. Table 2 summarizes the model sensitivity tests done for this study, including names for the runs used throughout this paper.

5.1. Effects of Shape

To constrain the likely effects of ice crystal shape on the evolution of TTL cirrus, we ran a SAM simulation assuming oblate spheroidal shape for the fall speed and growth rate calculations and hexagonal plate shape for the longwave radiative absorption, both with aspect ratios of 6. We call this the Oblate-Full case. To identify the physical mechanisms responsible for the effects of shape, we also did experiments in which the fall speed, growth rate, and LW radiative absorption were changed in various combinations. These include the Oblate Fall Speed and Oblate Growth Rate cases, which assumed spheroidal shape for fall speed and growth rate only, respectively, and the Oblate Microphysics case, which assumed spheroidal shape for both fall speed and growth rate but still assumed spheres for the LW absorption.

We also did analogous runs involving prolate spheroids instead of oblate spheroids, with hexagonal columnar shape assumed for the radiation in the "Prolate-Full" case. The results of the oblate and prolate cases are very similar to each other, because oblate and prolate spheroids (or plates and columns) are similar to each other in terms of their effects on each of the physical processes (see Figures 2, 3 and 4).

To understand the effects of shape on the cloud evolution, we show time series of domain-integrated quantities, including the altitude of the center of cloud ice mass and the total cloud ice mass for each of these cases, in Figure 5.

The center of mass rises monotonically with time in each case. This is due to a combination of the clouds being lifted by the radiatively induced circulation and the development of small-scale convection at the cloud top. The difference between the Oblate Growth Rate and Control cases (Figure 5a) shows that changing the growth rate to the spheroidal

calculation has a negligible effect on the center of mass for most of the simulation. The Oblate Fall Speed case shows that assuming spheroidal shape for fall speeds results in a higher center of mass at all elapsed times. A higher cloud center of mass is consistent with expectations because spheroids have reduced fall speeds (Figure 2). The Oblate-Microphysics case is very similar to the Oblate Fall Speed case in terms of the center of mass. Similar results are seen in the prolate spheroid cases (Figure 5c). Therefore, we attribute the effect of microphysics on the center of mass mostly to the slower fall speeds of non-spherical crystals.

Comparing the Oblate-Full case to the Oblate Microphysics case (or comparing the analogous prolate cases) gives insight into the role of radiation, since the only difference between these cases is the greater absorption by non-spherical crystals. Comparing these two cases to the Control case shows that microphysics is responsible for about 60% of the center of mass increase in the Oblate-Full or Prolate-Full case relative to the Control case, and radiation is responsible for the remaining 40%. The radiative heating of the cloud is stronger in the runs using the non-spherical absorption coefficients, and this additional heating induces stronger updrafts. Plots of the w field at 6 hours from the various cases (not shown) indicate that the updrafts are in fact stronger in simulations including the non-spherical radiation coefficients.

The total ice mass time series (Figures 5b and 5d) in all of the simulations share several features. There is an initial decline in ice mass at the beginning of the simulations, which can be attributed to RH_i decreases arising from local diabatic heating while the radiatively induced circulation is spinning up (see Section 6.1). After a minimum at about 9 hours, there is a rebound in the ice mass, which peaks at about 18 hours. After that peak, there

is a sustained decline in the total ice mass, and by 48 hours, the cloud has lost about 30% of its mass. This is different from the simulations of *Dinh et al.* [2010], who found a continued rise in cloud ice mass during the second day (see their Figure 8a). Such a discrepancy is surprising because the two studies had the same model resolution and initial conditions, and similar microphysics and radiation schemes. However, different models were used in the two studies (SAM in this study vs. Meso06 previously), with different bin microphysics schemes (*Dinh and Durran* [2012] here vs. *Chen and Lamb* [1994] previously) and changes to the fall speed calculation and LW absorption coefficients for spheres (see Sections 3.1 and 4.1), so we should not expect our control simulation to exactly match that of *Dinh et al.* [2010].

Overall, the total mass of thin TTL cirrus, at least for small (3 micron radius spherical equivalent) ice crystals, does not appear to be very sensitive to the shape of the ice crystals. At this mass, spheroids with an aspect ratio of 6 have about 1/3 slower fall speeds, 60% greater rate of mass growth or loss by deposition or sublimation, and 10% greater radiative absorption relative to spheres. This amounts to a 12% lower total ice mass at 48 hours in the oblate cases, and a slightly smaller difference in the prolate cases. By contrast, *Dinh et al.* [2010] found much greater declines in ice mass at 48 hours from increasing the initial ice crystal size to 8.8 μm or lowering RH_i of the cloud edge region to 80%, suggesting that ice crystal size and environmental humidity are much stronger controls on the cloud ice mass in subvisible TTL cirrus than ice crystal shape. As for the ice center of mass, the Oblate-Full and Prolate-Full cases have about 30% greater lofting at 48 hours than the Control case, but this is only about 65 meters, which may not be very dynamically important.

While ice crystal shape may not be very important to the cloud evolution, the sensitivity to the individual physical processes nonetheless provides interesting insights into the way these clouds are maintained. The shape effects on fall speed, growth rate and radiative absorption each have the potential to either encourage or discourage ice crystal growth, and these effects compete with each other.

In terms of microphysics, slower fall speeds for spheroids can either encourage or discourage ice crystal growth by preventing individual ice crystals from entering either subsaturated or supersaturated environments, respectively. As for growth rate, the magnitude of $\mathrm{d}m/\mathrm{d}t$ is greater for spheroids than for spheres (Figure 3), which implies that ice crystals grow faster in a supersaturated environment but shrink faster in a subsaturated environment. The Oblate and Prolate Growth Rate cases are very similar to the Control case, likely due to compensation between these effects or ice growth being limited by available water vapor if the cloud structure and dynamics do not change. The difference between the Control and Oblate Microphysics cases, especially towards the end, does not appear to be the sum of the differences between the Control case and the Oblate Fall Speed and Oblate Growth Rate cases, and a similar result is seen in the prolate cases. This indicates that the effects of non-spherical shape on fall speed and growth rate interact in complex, nonlinear ways and should not be assumed to be additive.

As for the radiative absorption, the Oblate-Full case curve in Figure 5b shows that using the non-spherical absorption coefficients, and therefore increasing the radiative absorption, results in less total ice mass at all times relative to the Oblate Microphysics case. This is a seemingly paradoxical result, because in the absence of radiative heating, there are no updrafts to maintain the cloud against sedimentation and the cloud dissipates. However,

besides strengthening updrafts, increased radiative heating also has the potential to reduce RH_i by increasing the temperature locally, an effect which competes with the additional moisture convergence and adiabatic cooling caused by stronger updrafts. The robustness and causes of this effect are further explored in Sections 5.2 and 6.1.

5.2. Additional Sensitivity Tests

5.2.1. Zero fall speed test

It may seem surprising that reducing ice crystal fall speeds by about 1/3 by assuming spheroids with aspect ratios of 6 only resulted in about a 40 meter increase in the center of cloud ice mass at 48 hours. Figure 6 shows the center of mass as a function of time in the Control case, the Oblate Fall Speed case, and a Zero Fall Speed case in which sedimentation was turned off. In the Zero Fall Speed case, the cloud is lofted by the radiative heating so that, at 48 hours, the center of mass is roughly 150 m higher than in the Control case. The center of mass in the Spheroid Fall Speed case is about a third of the way between the control and zero fall speed cases.

5.2.2. Radiative absorption multiplier tests

In Section 5.1 we found that switching from spherical ice crystals to spheroids increases the cloud radiative absorption and reduces the total ice cloud mass. This seems paradoxical because the circulation induced by the radiative absorption is responsible for the cloud being able to maintain itself against sedimentation. To further examine this result, we made more extreme changes to the radiative absorption while keeping the ice crystal shape fixed as spheres. We ran one case with the LW absorption doubled relative to the Control case (Double LW Absorption), one case with the LW absorption halved relative to the Control case (Half LW Absorption), one case with the SW absorption set to zero

(Zero SW Absorption), and one case with both the SW and LW absorption set to zero (Zero Radiative Absorption).

Plots of the center of ice mass for these cases (Figure 7a) show that in general, the greater the radiative absorption, the more the cloud is lofted over time. This is expected given that the radiative absorption is responsible for the updrafts that lift the cloud. With all radiative absorption shut off, the center of mass drops nearly linearly with time as the ice crystals slowly sediment. The Zero SW Absorption case is very similar to the Control case, indicating that the shortwave absorption is not very important.

The total ice mass plots (Figure 7b) confirm the apparently paradoxical result from the previous section that more radiative absorption results in less total ice mass, with the exception of the run with all radiative absorption turned off. With no radiative absorption, the total ice mass begins to decline as the ice crystals fall into the subsaturated region below the cloud's original location, and there is no circulation to counteract this effect. Therefore, radiative absorption is necessary to maintain the cloud in the absence of large-scale motions. The other runs indicate that there is an optimum amount of radiative absorption that maximizes the peak ice cloud mass in the simulation; after that optimum is passed, additional absorption lowers the peak cloud ice mass, as well as shifting the peak to earlier times.

6. Discussion

6.1. Role of Radiative Heating

To better understand the physical reasons for the inverse relationship between radiative absorption and ice mass, we show contour plots of the ice mass concentration, supersaturation ratio with respect to ice, and perturbation temperature in the Control and Double

LW Absorption cases (Figures 8 and 9). Figure 8 is at $t = 6$ hours, during the model spin-up period, while Figure 9 is at $t = 36$ hours, after the circulation has matured. As in *Dinh et al.* [2010], the cloud spreads out at the top and narrows at the base due to the radiatively induced circulation, and small-scale convection develops at the cloud top. Animations of these variables available in the online supplement show the full evolution of the cloud.

One might suppose that the initial decline in ice mass in the Control case was due to ice crystals sedimenting into the subsaturated region below the cloud, but the lack of such a decline in the Zero Radiative Absorption case (Figure 7b) shows that radiative heating must be directly involved in this decline in the other cases. The stronger the radiative heating, the greater the initial decline in ice mass. The mechanism for this effect is evident in Figure 8: doubling the radiative absorption raises the temperature and lowers RH_i in the center of the cloud, where the ice mass concentration is greatest.

To understand why stronger radiative heating inhibits ice growth after the circulation has spun up, we must examine the temperature and humidity fields to the sides of the cloud, both early and late in the simulation. Stronger heating leads to higher temperatures and lower RH_i well out to the sides of the cloud, due to greater adiabatic compression from the stronger circulation. The sides of the cloud are the regions from which moisture is drawn in order to sustain growth of ice crystals in the cloud [*Dinh et al.*, 2010], so lower RH_i there would inhibit the growth of ice crystals once the circulation has spun up. Indeed, at 36 hours (Figure 9), the center of the lower portion of the cloud, where moisture converges, is narrower and has much less cloud ice mass in the Double LW Absorption case than in the Control case.

Another mechanism by which stronger radiative heating limits the eventual cloud growth is that, as the entire cloud is lofted by the stronger circulation, it rises into the region above the original cloud top that was initially set at 80% RH_i. Also, the cloud top convection develops earlier in the simulation in the Double LW Absorption case, likely leading to more dry air being entrained into the cloud from above and thereby limiting the growth of ice in the uppermost part of the cloud.

6.2. Ice crystal size distributions

Dinh et al. [2012] found that ice crystal size distributions similar to observations could be obtained by retroactively converting spheres to columns or plates in their model output, but since these crystals were treated as spheres during the simulation, they were not able to show that such large crystals could actually be maintained in the modeled cloud without falling out. Now that we have modified the model to explicitly simulate non-spherical crystals, it is useful to revisit the comparison of modeled to observed size distributions. Figure 10 shows ice crystal size distributions at 24 and 48 hours in the Control, Oblate-Full and Prolate-Full cases, as well as observed size distributions from TTL cirrus over the Eastern Pacific [*Lawson et al.*, 2008]. The x-axis in these plots is length (diameter for spheres, major axis for spheroids), rather than mass, because microphysical observations of ice crystals typically measure the lengths of the crystals along their maximum dimension.

At 24 hours, our modeled size distribution in the spherical case is narrow compared with observations, with a peak at about 6 μm in diameter that has an order of magnitude more crystals than the observations at that size. This is because the modeled size distribution began as a delta function, with all of the ice crystals having a diameter of 6.0 μm. Switching to oblate or especially prolate spheroids shifts the size distribution to

the right but does not affect the spread, producing a greater number of large crystals but fewer small crystals than the spherical case.

At 48 hours in the three modeled cases, small ice crystals have become more numerous as average-size crystals have shrunk. Ice crystal numbers in the three bins larger than the modal size have been largely maintained, and have in fact increased in the second and third bin above the mode. The prolate spheroid case overestimates observed concentrations for crystals between 10 and 30 microns in length by almost two orders of magnitude, but the smaller concentrations at these sizes in the other cases suggests that a more realistic size distribution could be obtained by using a combination of spheres, oblate spheroids and prolate spheroids, or by allowing the aspect ratio to vary as ice crystals grow. Overall, our model is capable of maintaining ice crystals up to 40 microns in length to within an order of magnitude of the concentrations observed by *Lawson et al.* [2008].

The differences in the modeled size distributions in the different cases are due to the chosen assumption about the geometry itself, and not to the effects of the shape on the rate of ice crystal mass growth. Figure 5b shows that the variation in the total ice mass between the different cases is less than about 12% between the different cases, but Figure 10 shows that the prolate spheroids are generally over 3 times larger than the spheres. This is simply due to the relative elongation of spheroids at constant mass.

7. Conclusions

We have incorporated calculations of fall speeds, growth rates, and longwave radiative absorption for non-spherical ice crystals, specifically oblate and prolate spheroids with aspect ratios of 6 (or plates and columns in the case of the radiation), into a cloud-resolving model suitable for conducting experiments with idealized, optically thin cirrus

in the tropical tropopause layer (TTL). Results are compared with control simulations that assumed only spherical crystals.

Spheroids with aspect ratios of 6 have slower fall speeds (Figure 2), faster rates of growth by deposition and shrinking by sublimation (Figure 3), and stronger radiative absorption (Figure 4) than equivalent-mass spheres. The results of the cloud-resolving model simulations show that these changes in the ice crystal habits do affect the time evolution of the cloud. However, while not entirely negligible, the effects of ice crystal shape appear to be relatively unimportant compared to other factors such as ice crystal mass or the humidity field surrounding the cloud.

While shape is not particularly important to cloud dynamics, our sensitivity tests provide insights into the physical mechanisms involved in the clouds' maintenance. Slower fall speeds and stronger radiative heating raise the center of mass of the cloud, while faster ice crystal growth and sublimation matter little for this quantity. The control simulation appears to be in a regime in which stronger radiative heating results in less ice mass, due to a combination of local diabatic heating in the cloud, adiabatic warming of the cloud source air, lofting of the cloud into a subsaturated region above its original position, and earlier onset of cloud top convection. The strong sensitivity of the cloud evolution to the amount of radiation it absorbs has implications for how thin TTL cirrus would behave in other situations. For example, in the case of a thin cirrus cloud located above a thicker cirrus cloud, the amount of longwave radiation reaching the thin cloud is much less, because the cloud top is much colder than the surface. We hypothesize that a thin cirrus cloud may actually exhibit more ice growth if located above a thicker cirrus than if isolated.

Caution should be used when extending our results to optically thicker cirrus. The dynamics of those clouds are affected by absorbed shortwave radiation [*Ackerman et al.*, 1988]. An analogous study of thicker cirrus would require a radiative transfer scheme that explicitly accounts for multiple scattering and the changing optical path with wavelength. Ice crystal shape would be expected to be more important for thick than for thin cirrus, because the larger ice crystals in thick cirrus have much greater fall speeds, so changes to those fall speeds would have a greater impact on the cloud dynamics.

Our results suggest that incorporating non-spherical ice crystal shapes has the potential to help make the modeled ice crystal size distributions more realistic. However, more work needs to be done in order to achieve this goal. Modeling a pre-existing, initially monodisperse cloud arbitrarily makes the ice crystal size distribution too narrow compared with observations. A better approach would be to return to the configuration of *Dinh et al.* [2012], in which the cloud was nucleated from aerosol droplets in an initial moist patch lifted by a large-scale wave. This simulation of the entire life cycle of the cloud provides for a better comparison between the modeled and observed size distributions. Also, the ice crystal shapes and size distributions in real TTL cirrus need to be better characterized using observations. The recently completed Airborne Tropical Tropopause Experiment [ATTREX; *Jensen et al.*, 2015] used the NASA Global Hawk unmanned aircraft to provide unprecedented observations of TTL cirrus over a wide temporal and spatial range. A thorough analysis of this dataset should provide a much improved understanding of the microphysics and dynamics of TTL cirrus.

Acknowledgments.

Model output and plotting scripts are available online at http://www.atmos.washington.edu/articles/Sensitivity_TTL_Cirrus_Shape_Absorption/. Requests for the specific microphysics and radiation schemes and parameterizations used in this paper should be directed to T. P. Ackerman at ackerman@atmos.washington.edu. A general version of the SAM model is available at http://rossby.msrc.sunysb.edu/~marat/SAM.html. RRTM is available at http://rtweb.aer.com/rrtm_frame.html. The T-Matrix code is available at http://www.giss.nasa.gov/staff/mmishchenko/t_matrix.html. The ice optical constants from Warren and Brandt [2008] are available at http://www.atmos.washington.edu/ice_optical_constants/.

This research was supported by the National Science Foundation (NSF) through grant ATM-0926996 and by the U.S. Department of Defense (DoD) through the National Defense Science and Engineering Graduate Fellowship (NDSEG) Program. This work was facilitated though the use of advanced computational, storage, and networking infrastructure provided by the Hyak supercomputer system at the University of Washington. Three anonymous reviewers provided comments which greatly helped to improve this manuscript. The authors are grateful to Tra Dinh, who provided valuable insights based on her own experience modeling TTL cirrus, and to Stephen Warren, who provided helpful suggestions for calculating the radiative properties of non-spherical ice crystals.

References

Ackerman, T. P., K.-N. Liou, F. P. Valero, and L. Pfister (1988), Heating rates in tropical anvils, *Journal of the Atmospheric Sciences*, *45*(10), 1606–1623.

Asano, S., and M. Sato (1980), Light scattering by randomly oriented spheroidal particles, *Applied Optics*, *19*(6), 962–974.

Asano, S., and G. Yamamoto (1975), Light scattering by a spheroidal particle, *Applied Optics*, *14*(1), 29–49.

Avramov, A., and J. Y. Harrington (2010), Influence of parameterized ice habit on simulated mixed phase Arctic clouds, *Journal of Geophysical Research: Atmospheres*, *115*(D3), D03205, doi:10.1029/2009JD012108.

Bi, L., P. Yang, G. W. Kattawar, B. A. Baum, Y. X. Hu, D. M. Winker, R. S. Brock, and J. Q. Lu (2009), Simulation of the color ratio associated with the backscattering of radiation by ice particles at the wavelengths of 0.532 and 1.064 μm, *Journal of Geophysical Research: Atmospheres*, *114*(D4), D00H08, doi:10.1029/2009JD011759.

Blossey, P. N., and D. R. Durran (2008), Selective monotonicity preservation in scalar advection, *Journal of Computational Physics*, *227*(10), 5160–5183, doi:http://dx.doi.org/10.1016/j.jcp.2008.01.043.

Böhm, H. P. (1989), A general equation for the terminal fall speed of solid hydrometeors, *Journal of the Atmospheric Sciences*, *46*, 2419–2427.

Bougeault, P. (1983), A non-reflective upper boundary condition for limited-height hydrostatic models, *Monthly Weather Review*, *111*, 420–429.

Chen, J.-P., and D. Lamb (1994), Simulation of cloud microphysical and chemical processes using a multicomponent framework. Part I: Description of the microphysical model, *Journal of the Atmospheric Sciences*, *51*(18), 2613–2630.

Cheng, W. Y. Y., T. Wu, and W. R. Cotton (2001), Large-eddy simulations of the 26 November 1991 FIRE II cirrus case, *Journal of the Atmospheric Sciences*, *58*, 1017–

1034.

Comstock, J. M., T. P. Ackerman, and G. G. Mace (2002), Ground-based lidar and radar remote sensing of tropical cirrus clouds at Nauru island: Cloud statistics and radiative impacts, *Journal of Geophysical Research: Atmospheres*, *107*(D23), AAC 16–1–AAC 16–14, doi:10.1029/2002JD002203.

Corti, T., B. P. Luo, Q. Fu, H. Vömel, and T. Peter (2006), The impact of cirrus clouds on tropical troposphere-to-stratosphere transport, *Atmospheric Chemistry and Physics*, *6*(9), 2539–2547, doi:10.5194/acp-6-2539-2006.

Dinh, T., and D. R. Durran (2012), A hybrid bin scheme to solve the condensation/evaporation equation using a cubic distribution function, *Atmospheric Chemistry and Physics*, *12*(2), 1003–1011, doi:10.5194/acp-12-1003-2012.

Dinh, T., and S. Fueglistaler (2014a), Microphysical, radiative and dynamical impacts of thin cirrus clouds on humidity in the tropical tropopause layer and lower stratosphere, *Geophysical Research Letters*, *41*, 6949–6955, doi:10.1002/2014GL061289.

Dinh, T., and S. Fueglistaler (2014b), Cirrus, transport and mixing in the tropical upper troposphere, *Journal of the Atmospheric Sciences*, *71*, 1339–1352.

Dinh, T., D. Durran, and T. Ackerman (2010), Maintenance of tropical tropopause layer cirrus, *Journal of Geophysical Research (Atmospheres)*, *115*, D02104, doi:10.1029/2009JD012735.

Dinh, T., D. R. Durran, and T. Ackerman (2012), Cirrus and water vapor transport in the tropical tropopause layer – Part 1: A specific case modeling study, *Atmospheric Chemistry and Physics*, *12*(20), 9799–9815, doi:10.5194/acp-12-9799-2012.

Dinh, T., S. Fueglistaler, D. Durran, and T. Ackerman (2014), Cirrus and water vapour transport in the tropical topopause layer – Part 2: Roles of ice nucleation and sedimentation, cloud dynamics, and moisture conditions, *Atmospheric Chemistry and Physics*, *14*, 12,225–12,236, doi:10.5194/acp-14-12225-2014.

Dinh, T. P. (2012), Cirrus and water vapor transport in the tropical tropopause layer, Ph.D. thesis, University of Washington, Seattle, WA, USA.

Durran, D. R., T. Dinh, M. Ammerman, and T. Ackerman (2009), The mesoscale dynamics of thin tropical tropopause cirrus, *Journal of the Atmospheric Sciences*, *66*(9), 2859 – 2873.

Dvortsov, V. L., and S. Solomon (2001), Response of the stratospheric temperatures and ozone to past and future increases in stratospheric humidity, *Journal of Geophysical Research: Atmospheres*, *106*(D7), 7505–7514, doi:10.1029/2000JD900637.

Fu, Q., P. Yang, and W. Sun (1998), An accurate parameterization of the infrared radiative properties of cirrus clouds for climate models, *Journal of Climate*, *11*, 2223–2237.

Fuchs, N. A. (1964), *The Mechanics of Aerosols*, Pergamon Press, New York, NY, USA.

Fueglistaler, S., A. E. Dessler, T. J. Dunkerton, I. Folkins, Q. Fu, and P. W. Mote (2009), Tropical tropopause layer, *Reviews of Geophysics*, *47*, RG1004.

Gettelman, A., P. M. d. F. Forster, M. Fujiwara, Q. Fu, H. Vmel, L. K. Gohar, C. Johanson, and M. Ammerman (2004), Radiation balance of the tropical tropopause layer, *Journal of Geophysical Research: Atmospheres*, *109*(D7), D07103, doi:10.1029/2003JD004190.

Gierens, K. M. (1994), The influence of radiation on the diffusional growth of ice crystals, *Beitr. Phys. Atmosph.*, *67*(3), 181–193.

Grenfell, T. C., and S. G. Warren (1999), Representation of a nonspherical ice particle by a collection of independent spheres for scattering and absorption of radiation, *Journal of Geophysical Research: Atmospheres*, *104*(D24), 31,697–31,709, doi: 10.1029/1999JD900496.

Grenfell, T. C., S. P. Neshyba, and S. G. Warren (2005), Representation of a nonspherical ice particle by a collection of independent spheres for scattering and absorption of radiation: 3. hollow columns and plates, *Journal of Geophysical Research: Atmospheres*, *110*(D17), D17203, doi:10.1029/2005JD005811.

Jensen, E., and L. Pfister (2004), Transport and freeze-drying in the tropical tropopause layer, *Journal of Geophysical Research: Atmospheres*, *109*(D2), D02207, doi:10.1029/2003JD004022.

Jensen, E. J., O. B. Toon, L. Pfister, and H. B. Selkirk (1996), Dehydration of the upper troposphere and lower stratosphere by subvisible cirrus clouds near the tropical tropopause, *Geophysical Research Letters*, *23*(8), 825–828, doi:10.1029/96GL00722.

Jensen, E. J., L. Pfister, T. V. Bui, P. Lawson, B. Baker, Q. Mo, D. Baumgardner, E. M. Weinstock, J. B. Smith, E. J. Moyer, T. F. Hanisco, D. S. Sayres, J. M. S. Clair, M. J. Alexander, O. B. Toon, and J. A. Smith (2008), Formation of large ($\simeq$ 100 μm) ice crystals near the tropical tropopause, *Atmospheric Chemistry and Physics*, *8*(6), 1621–1633, doi:10.5194/acp-8-1621-2008.

Jensen, E. J., L. Pfister, and O. B. Toon (2011), Impact of radiative heating, wind shear, temperature variability, and microphysical processes on the structure and evolution of thin cirrus in the tropical tropopause layer, *Journal of Geophysical Research: Atmospheres*, *116*(D12), D12,209, doi:10.1029/2010JD015417.

Jensen, E. J., L. Pfister, D. E. Jordan, T. V. Bui, R. Ueyama, H. B. Singh, T. Thornberry, A. W. Rollins, R.-S. Gau, D. W. Fahey, K. H. Rosenlof, J. W. Elkins, G. S. Diskin, J. P. DiGangi, R. P. Lawson, S. Woods, E. L. Atlas, M. A. Navarro Rodriquez, S. C. Wofsy, J. Pittman, C. G. Bardeen, O. B. Toon, B. C. Kindel, P. A. Newman, M. J. MgGill, D. L. Hlavka, L. R. Lait, M. R. Schoeberl, J. W. Bergman, H. B. Selkirk, M. J. Alexander, J.-E. Kim, B. H. Lim, J. Stutz, and K. Pfeilsticker (2015), The NASA Airborne Tropical TRopopoause EXperiment (ATTREX): High-altitude aircraft measurements in the tropical western Pacific, *Bulletin of the American Meteorological Society*, doi: 10.1175/BAMS-D-14-00263.1, in press.

Khairoutdinov, M. F., and D. A. Randall (2003), Cloud resolving modeling of the ARM summer 1997 IOP: Model formulation, results, uncertainties, and sensitivities., *Journal of the Atmospheric Sciences*, *60*(4), 607–625.

Klemp, J. B., and D. R. Durran (1983), An upper boundary condition permitting internal gravity wave radiation in numerical mesoscale models, *Monthly Weather Review*, *111*, 430–444.

Lamb, D., and J. Verlinde (2011), *Physics and Chemistry of Clouds*, 584 pp., Cambridge University Press, Cambridge, UK.

Lawson, R. P., B. Pilson, B. Baker, Q. Mo, E. Jensen, L. Pfister, and P. Bui (2008), Aircraft measurements of microphysical properties of subvisible cirrus in the tropical tropopause layer, *Atmospheric Chemistry and Physics*, *8*(6), 1609–1620, doi:10.5194/acp-8-1609-2008.

Lee, J., P. Yang, A. E. Dessler, B.-C. Gao, and S. Platnick (2009), Distribution and radiative forcing of tropical thin cirrus clouds, *Journal of the Atmospheric Sciences*, *66*,

3721–3731.

Mace, G. G., Q. Zhang, M. Vaughan, R. Marchand, G. Stephens, C. Trepte, and D. Winker (2009), A description of hydrometeor layer occurrence statistics derived from the first year of merged Cloudsat and CALIPSO data, *Journal of Geophysical Research: Atmospheres*, *114*(D8), D00A26, doi:10.1029/2007JD009755.

Magee, N., A. M. Moyle, and D. Lamb (2006), Experimental determination of the deposition coefficient of small cirrus-like ice crystals near -50 °C, *Geophysical Research Letters*, *33*(17), L17813, doi:10.1029/2006GL026665.

Mishchenko, M. I., and L. D. Travis (1998), Capabilities and limitations of a current FORTRAN implementation of the T-matrix method for randomly oriented, rotationally symmetric scatterers, *Journal of Quantitative Spectroscopy and Radiative Transfer*, *60*(3), 309 – 324, doi:http://dx.doi.org/10.1016/S0022-4073(98)00008-9.

Mlawer, E. J., S. J. Taubman, P. D. Brown, M. J. Iacono, and S. A. Clough (1997), Radiative transfer for inhomogeneous atmospheres: RRTM, a validated correlated-k model for the longwave, *Journal of Geophysical Research: Atmospheres*, *102*(D14), 16,663–16,682, doi:10.1029/97JD00237.

Neshyba, S. P., T. C. Grenfell, and S. G. Warren (2003), Representation of a nonspherical ice particle by a collection of independent spheres for scattering and absorption of radiation: 2. hexagonal columns and plates, *Journal of Geophysical Research: Atmospheres*, *108*(D15), 4448, doi:10.1029/2002JD003302.

Podglajen, A., R. Plougonven, A. Hertzog, and B. Legras (2015), A modelling case study of a large-scale cirrus in the tropical tropopause layer, *Atmospheric Chemistry and Physics Discussions*, *15*(21), 31,089–31,131, doi:10.5194/acpd-15-31089-2015.

Pruppacher, H. R., and J. D. Klett (1978), *Microphysics of Clouds and Precipitation*, 1st ed., D. Reidel, Dotrecht, Holland.

Sölch, I., and B. Kärcher (2011), Process-oriented large-eddy simulations of a midlatitude cirrus cloud system based on observations, *Quarterly Journal of the Royal Meteorological Society*, *137*(655), 374–393, doi:10.1002/qj.764.

Solomon, S., R. R. Garcia, F. S. Rowland, and D. J. Wuebbles (1986), On the depletion of Antarctic ozone, *Nature*, *321*, 755–758.

Solomon, S., K. Rosenlof, R. W. Portmann, J. S. Daniel, S. M. Davis, T. J. Sanford, and G.-K. Plattner (2010), Contributions of stratospheric water vapor to decadal changes in the rate of global warming, *Science*, *327*, 1219–1223.

Stamnes, K., S.-C. Tsay, W. Wiscombe, and K. Jayaweera (1988), Numerically stable algorithm for discrete-ordinate-method radiative transfer in multiple scattering and emitting layered media, *Appl. Opt.*, *27*(12), 2502–2509, doi:10.1364/AO.27.002502.

Stamnes, K., S.-C. Tsay, and I. Laszlo (2000), DISORT, a general-purpose Fortran program for discrete-ordinate-method radiative transfer in scattering and emitting layered media: Documentation of methodology, *Tech. rep.*, NASA, version 1.1.

Taylor, J. R., W. J. Randel, and E. J. Jensen (2011), Cirrus cloud-temperature interactions in the tropical tropopause layer: a case study, *Atmospheric Chemistry and Physics*, *11*(19), 10,085–10,095, doi:10.5194/acp-11-10085-2011.

Toon, O. B., and T. P. Ackerman (1981), Algorithms for the calculation of scattering by stratified spheres, *Appl. Opt.*, *20*(20), 3657–3660, doi:10.1364/AO.20.003657.

Ueyama, R., E. J. Jensen, L. Pfister, G. S. Diskin, T. P. Bui, and J. M. Dean-Day (2014), Dehydration in the tropical tropopause layer: A case study for model evaluation using

aircraft observations, *Journal of Geophysical Research: Atmospheres*, *119*(9), 5299–5316, doi:10.1002/2013JD021381, 2013JD021381.

Ulanowski, Z., P. Connolly, M. Flynn, M. Gallagher, A. Clarke, and E. Hesse (2004), Using ice crystal analogues to validate cloud ice parameter retrievals from the cpi ice spectrometer data, in *14th International Conference on Clouds and Precipitation, Bologna, Italy*.

Um, J., and G. M. McFarquhar (2011), Dependence of the single-scattering properties of small ice crystals on idealized shape models, *Atmospheric Chemistry and Physics*, *11*(7), 3159–3171, doi:10.5194/acp-11-3159-2011.

Virts, K. S., and J. M. Wallace (2010), Annual, interannual, and intraseasonal variability of tropical tropopause transition layer cirrus, *Journal of the Atmospheric Sciences*, *67*, 3097–3112.

Wang, P.-H., P. Minnis, M. P. McCormick, G. S. Kent, and K. M. Skeens (1996), A 6-year climatology of cloud occurrence frequency from Stratospheric Aerosol and Gas Experiment II observations (1985-1990), *Journal of Geophysical Research*, *101*(D23), 29,407–29,429.

Warren, S. G., and R. E. Brandt (2008), Optical constants of ice from the ultraviolet to the microwave: A revised compilation, *Journal of Geophysical Research: Atmospheres*, *113*(D14), D14220, doi:10.1029/2007JD009744.

Winker, D. M., and C. R. Trepte (1998), Laminar cirrus observed near the tropical tropopause by LITE, *Geophysical Research Letters*, *25*(17), 3351–3354, doi:10.1029/98GL01292.

Wu, T., W. R. Cotton, and W. Y. Y. Cheng (2000), Radiative effects on the diffusional growth of ice particles in cirrus clouds, *Journal of the Atmospheric Sciences*, *57*, 2892–2904.

Yang, P., L. Bi, B. A. Baum, K.-N. Liou, G. W. Kattawar, M. I. Mishchenko, and B. Cole (2013), Spectrally consistent scattering, absorption, and polarization properties of atmospheric ice crystals at wavelengths from 0.2 to 100 μm, *Journal of the Atmospheric Sciences*, *70*, 330–347.

Zhang, C., and J. Y. Harrington (2015), The effects of surface kinetics on crystal growth and homogeneous freezing in parcel simulations of cirrus, *Journal of the Atmospheric Sciences*, *72*, 2929–2946.

Table 1. Parameterized absorption cross sections (m^2) in the longwave for spheres (see Section 4), for plates and columns with aspect ratios of 6 using the method of *Neshyba et al.* [2003], and in the shortwave for spheres (*Durran et al.* [2009], with subsequent extension to sizes larger than 13.0 microns). Sizes expressed in terms of radius of equivalent-volume sphere, r_V.

r_V (μm)	LW (spheres)	LW (plates)	LW (columns)	SW (spheres)
1.0	6.65×10^{-13}	6.51×10^{-13}	6.51×10^{-13}	1.0×10^{-14}
2.2	6.81×10^{-12}	7.12×10^{-12}	7.12×10^{-12}	1.0×10^{-13}
3.4	2.23×10^{-12}	2.54×10^{-11}	2.53×10^{-11}	3.0×10^{-13}
4.6	4.76×10^{-11}	5.88×10^{-11}	5.85×10^{-11}	6.1×10^{-13}
5.8	8.22×10^{-11}	1.08×10^{-10}	1.08×10^{-10}	1.0×10^{-12}
7.0	1.27×10^{-10}	1.74×10^{-10}	1.73×10^{-10}	1.5×10^{-12}
8.2	1.79×10^{-10}	2.56×10^{-10}	2.54×10^{-10}	2.2×10^{-12}
9.4	2.42×10^{-10}	3.52×10^{-10}	3.48×10^{-10}	3.0×10^{-12}
10.6	3.10×10^{-10}	4.64×10^{-10}	4.59×10^{-10}	4.1×10^{-12}
11.8	3.91×10^{-10}	5.93×10^{-10}	5.85×10^{-10}	5.4×10^{-12}
13.0	4.79×10^{-10}	7.34×10^{-10}	7.24×10^{-10}	6.4×10^{-12}
15.5	7.00×10^{-10}	1.08×10^{-9}	1.06×10^{-9}	1.0×10^{-11}
22.9	1.56×10^{-9}	2.47×10^{-9}	2.44×10^{-9}	2.6×10^{-11}
33.8	3.39×10^{-9}	5.54×10^{-9}	5.44×10^{-9}	6.8×10^{-11}
50.0	7.32×10^{-9}	1.21×10^{-8}	1.19×10^{-8}	1.8×10^{-10}

Table 2. Summary of cloud-resolving model runs, including case labels used throughout this paper, and the shape assumptions used in the calculations of various physical processes. All spheroids, plates and columns assumed to have aspect ratios of 6.

Case	Fall Speed	Growth Rate	LW Absorption	SW Absorption
Control	Spheres	Spheres	Spheres	Spheres
Oblate Fall Speed	Oblate Spheroids	Spheres	Spheres	Spheres
Oblate Growth Rate	Spheres	Oblate Spheroids	Spheres	Spheres
Oblate Microphysics	Oblate Spheroids	Oblate Spheroids	Spheres	Spheres
Oblate-Full	Oblate Spheroids	Oblate Spheroids	Plates	Spheres
Prolate Fall Speed	Prolate Spheroids	Spheres	Spheres	Spheres
Prolate Growth Rate	Spheres	Prolate Spheroids	Spheres	Spheres
Prolate Microphysics	Prolate Spheroids	Prolate Spheroids	Spheres	Spheres
Prolate-Full	Prolate Spheroids	Prolate Spheroids	Columns	Spheres
Zero Fall Speed	0	Spheres	Spheres	Spheres
Double LW Absorption	Spheres	Spheres	Spheres$\times$2.0	Spheres
Half LW Absorption	Spheres	Spheres	Spheres$\times$0.5	Spheres
Zero SW Absorption	Spheres	Spheres	Spheres	0
Zero Radiative Absorption	Spheres	Spheres	0	0

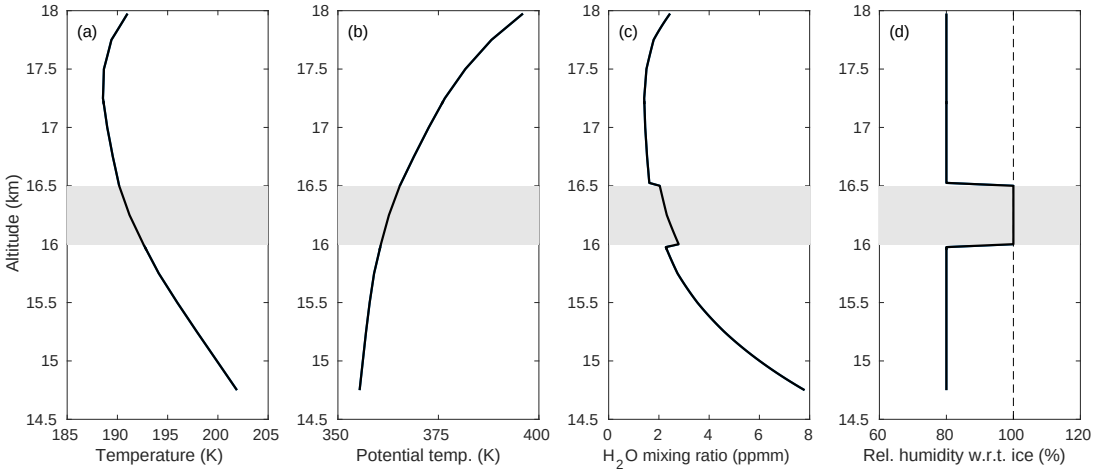

Figure 1. Initial profiles of temperature (a), potential temperature (b), water vapor mixing ratio (c), and relative humidity with respect to ice (d). The dashed line indicates saturation. The gray rectangle indicates the initial location of the cloud. At the beginning of these simulations, these quantities do not depend on x, although the ice number concentration does depend on x.

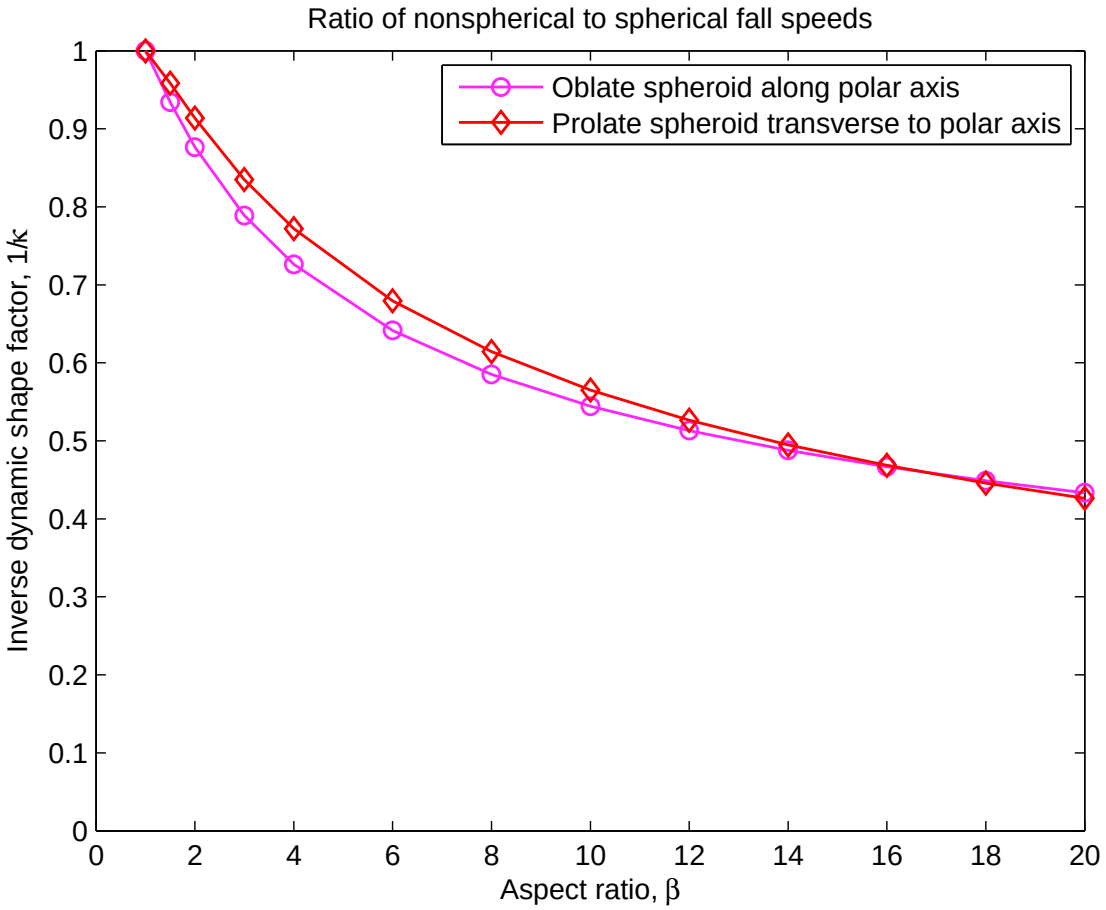

Figure 2. Ratios of the fall speeds of spheroidal particles to those of spherical particles of the same mass.

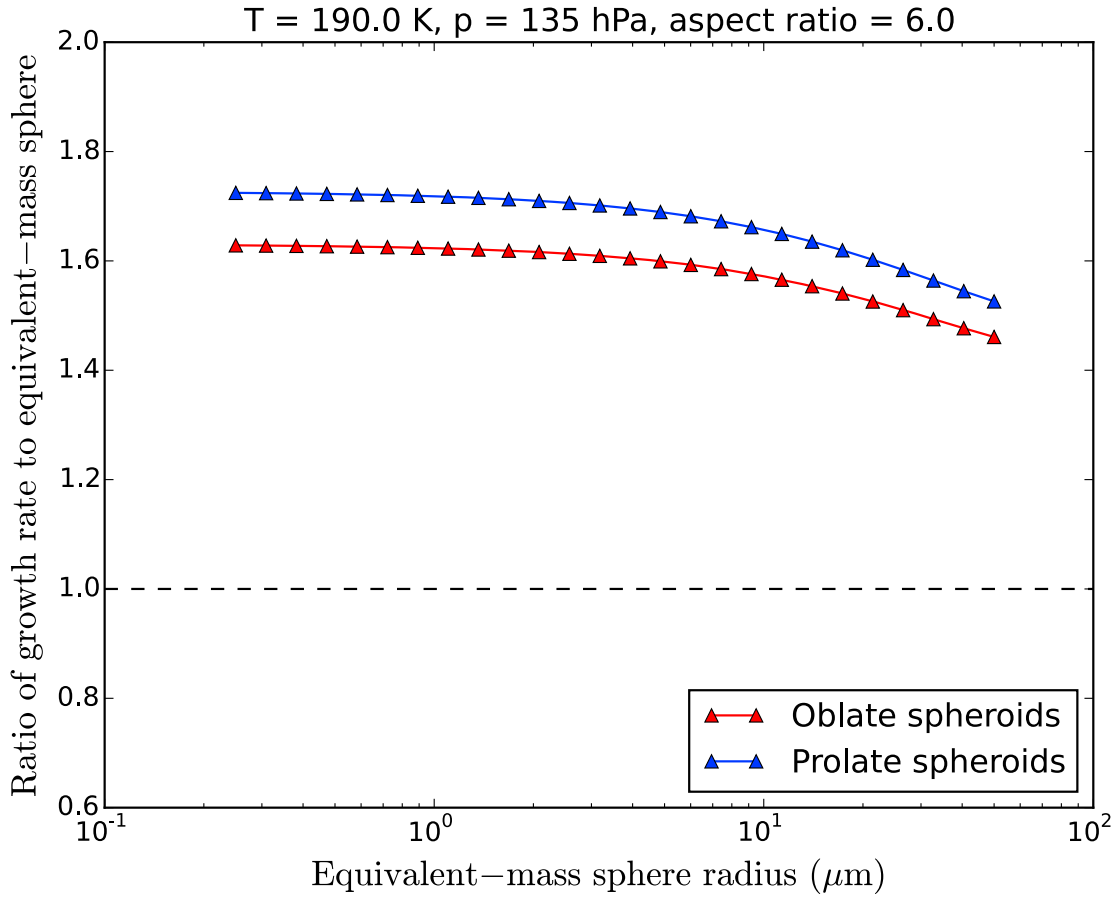

Figure 3. Ratios of mass growth rates for oblate (red) and prolate (blue) spheroids with aspect ratios of 6 to those for the equivalent-mass sphere, as a function of particle size; assumes a temperature of 190 K and a pressure of 135 hPa.

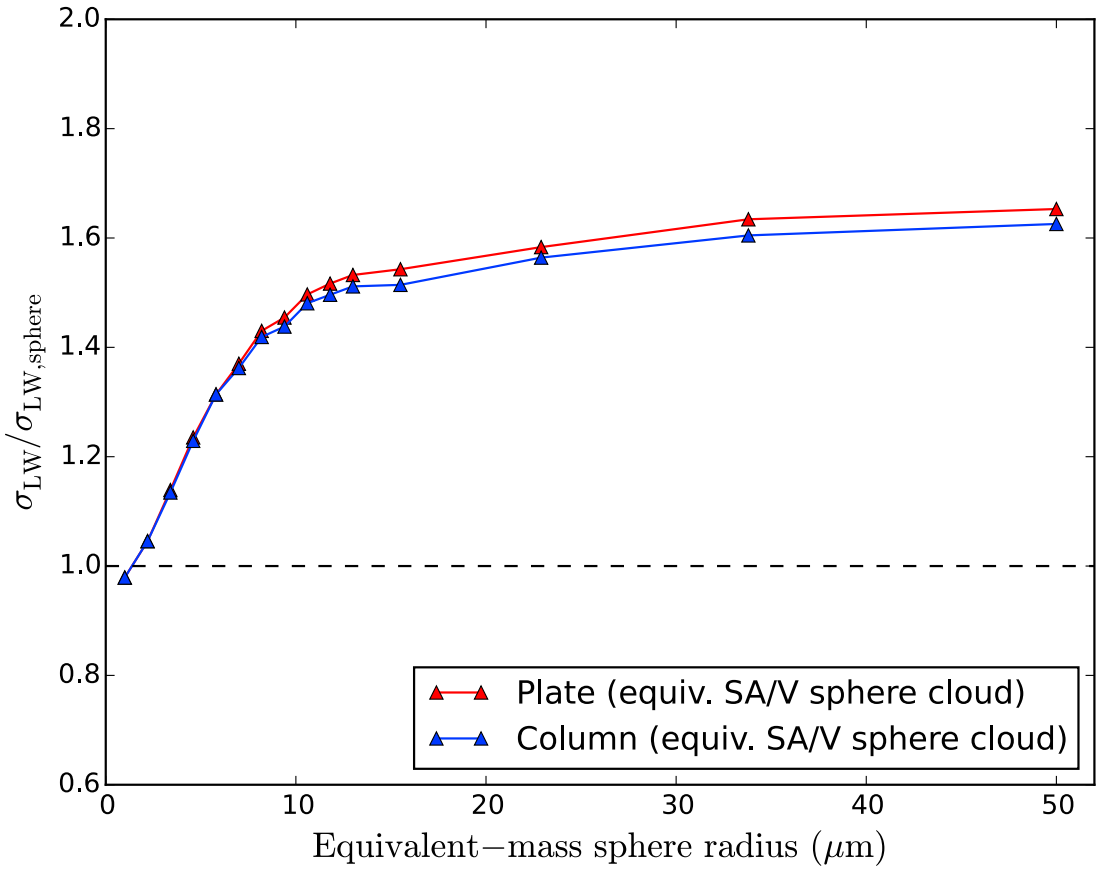

Figure 4. Ratios of the parameterized longwave absorption cross sections for columns and plates to those for spheres of equivalent mass, as a function of equivalent-mass sphere radius.

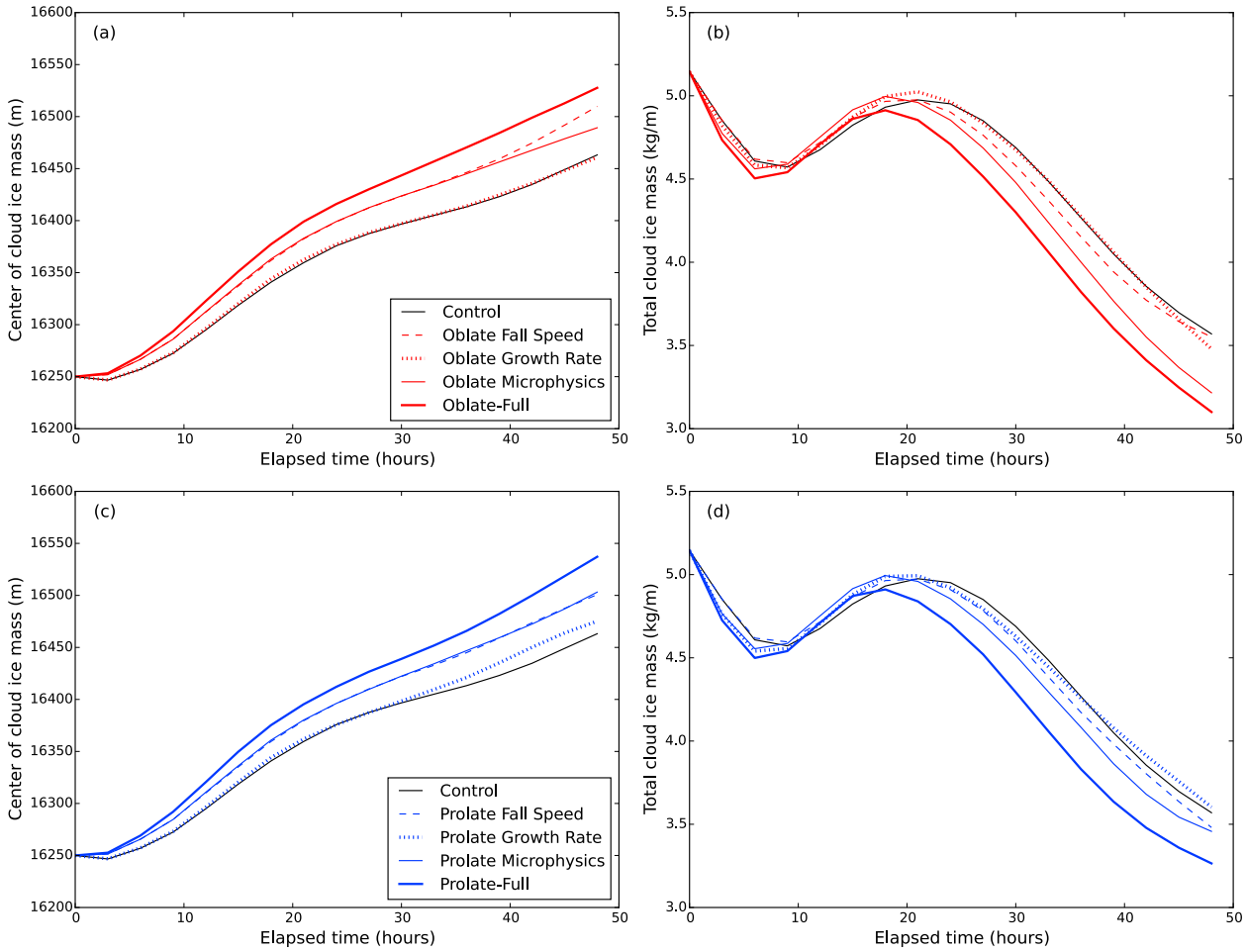

Figure 5. (a) Cloud ice center of mass and (b) domain-integrated ice mass in the Control (spherical) simulation and simulations assuming oblate spheroidal shape for microphysics and plate shape for radiation. (c) Cloud ice center of mass and (d) domain-integrated ice mass in the Control (spherical) simulation and simulations assuming prolate spheroidal shape for microphysics and columnar shape for radiation.

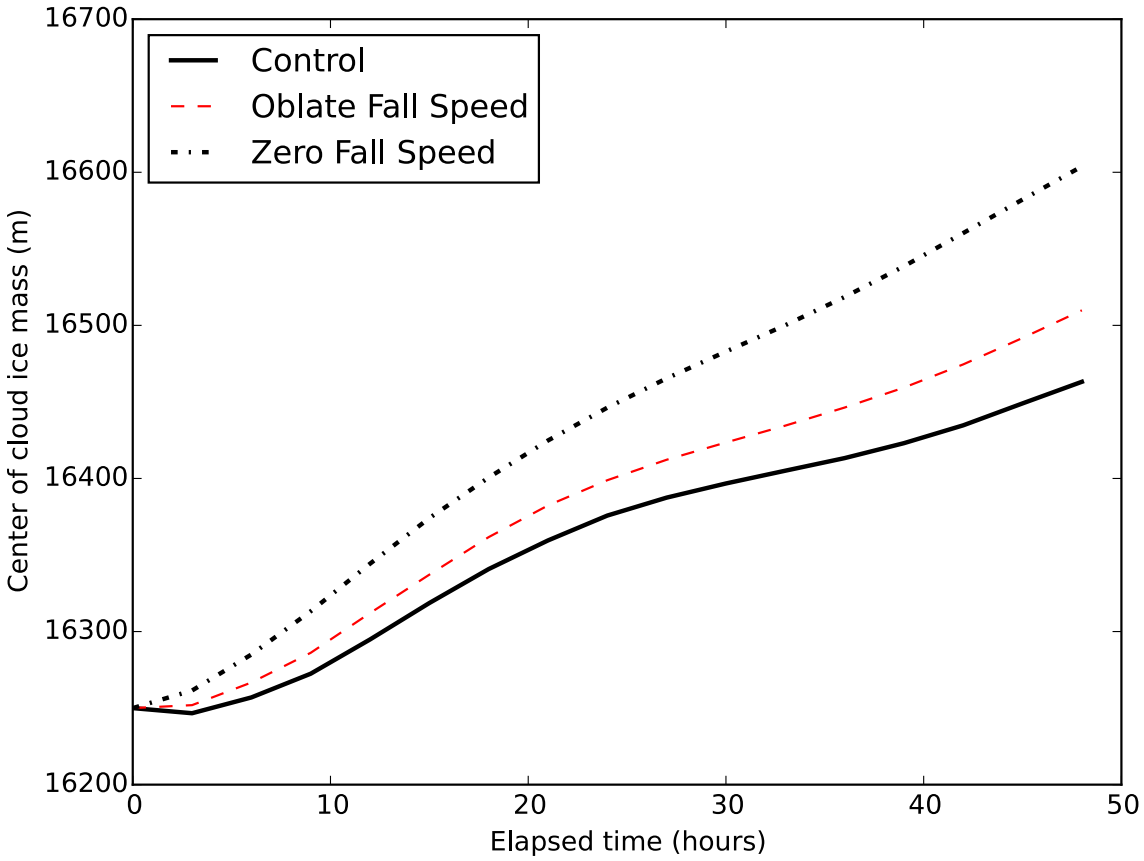

Figure 6. Center of cloud ice mass as a function of time in the Control case; the Oblate Fall Speed case, in which fall speeds were reduced by about 1/3; and the Zero Fall Speed case, in which sedimentation was turned off.

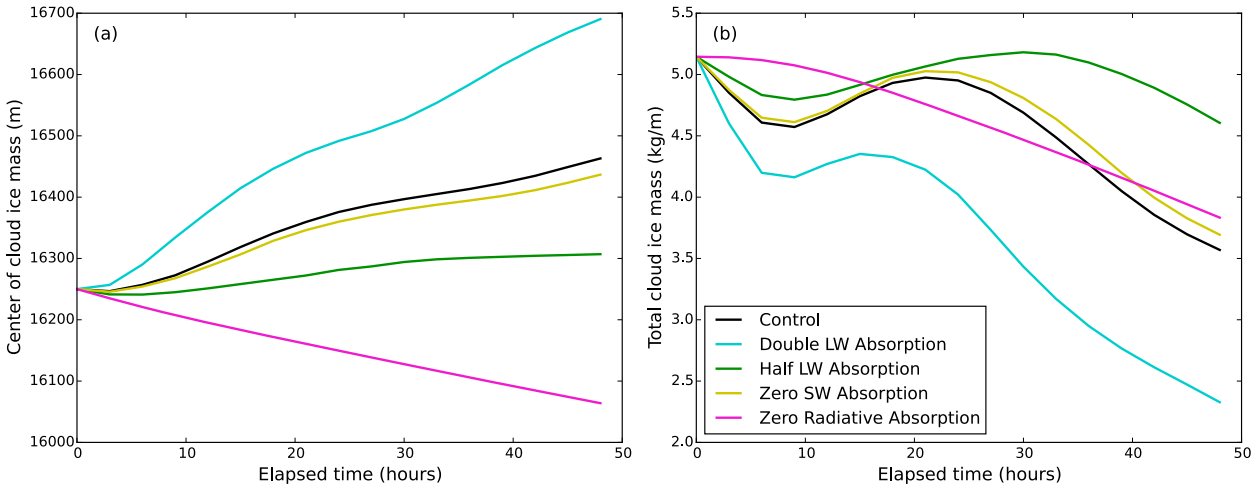

Figure 7. Cloud ice center of mass (a) and domain-integrated ice mass (b) in the Control simulation and sensitivity tests to changes in the SW and LW radiative absorption coefficients.

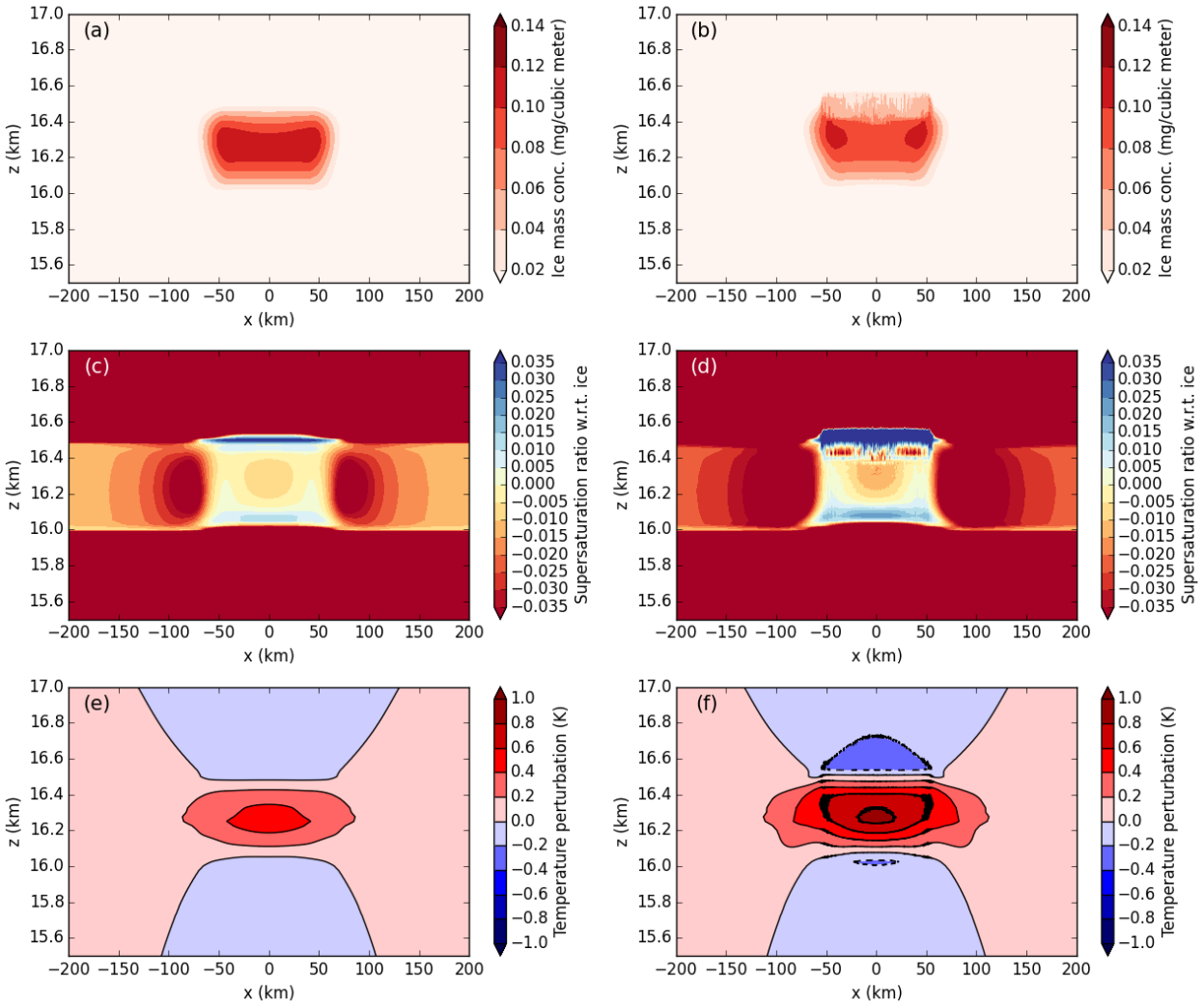

Figure 8. Contour plots at an elapsed time of 6 hours for ice mass concentration in the Control case (a) and the Double LW Absorption case (b), supersaturation ratio with respect to ice in the Control case (c) and the Double LW Absorption case (d), and temperature perturbation in the Control case (e) and the Double LW Absorption case (f). Note that the cloud is much wider and shallower than it appears given the roughly 270:1 vertical exaggeration in the plot window.

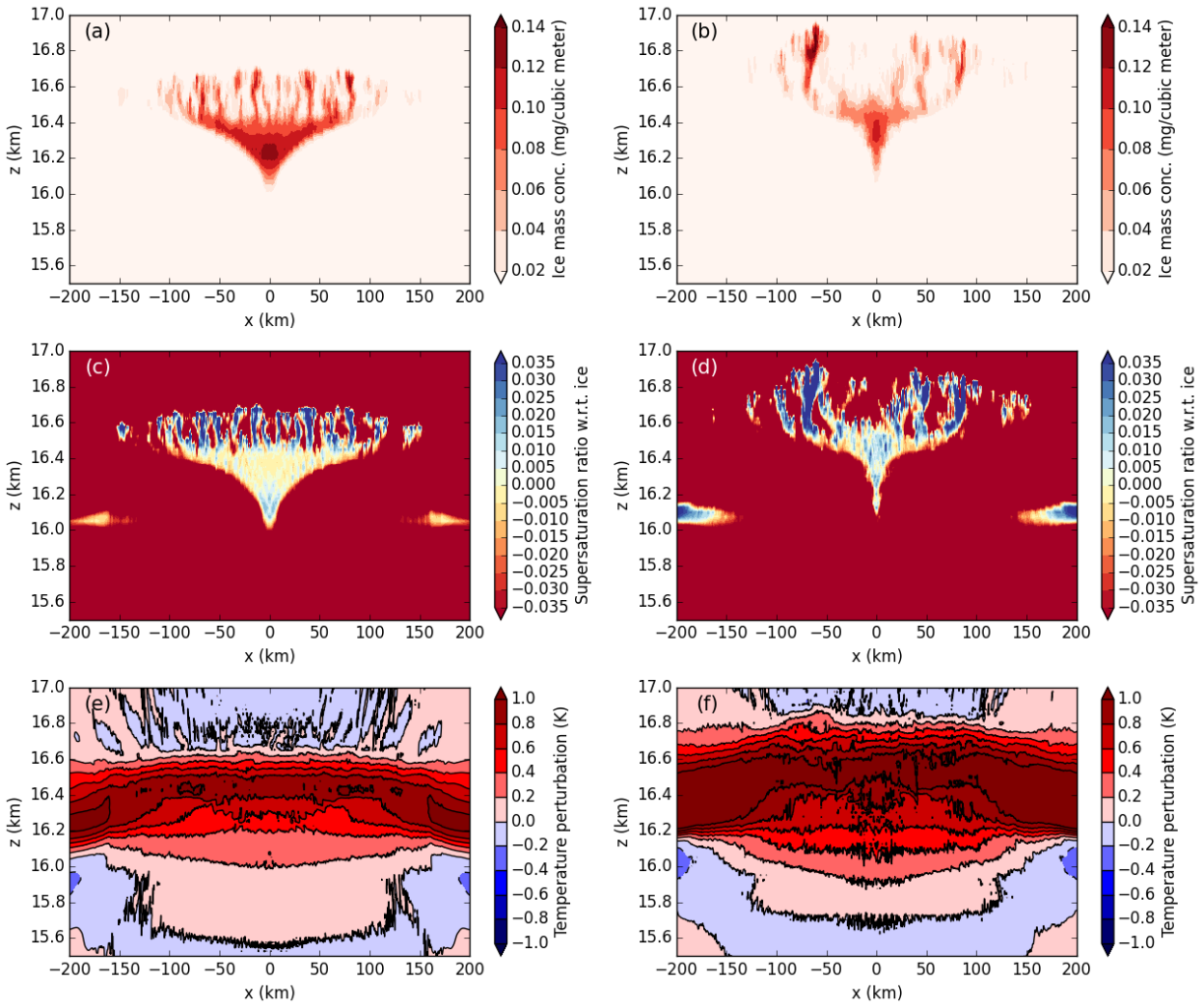

Figure 9. As in Figure 8 but at an elapsed time of 36 hours.

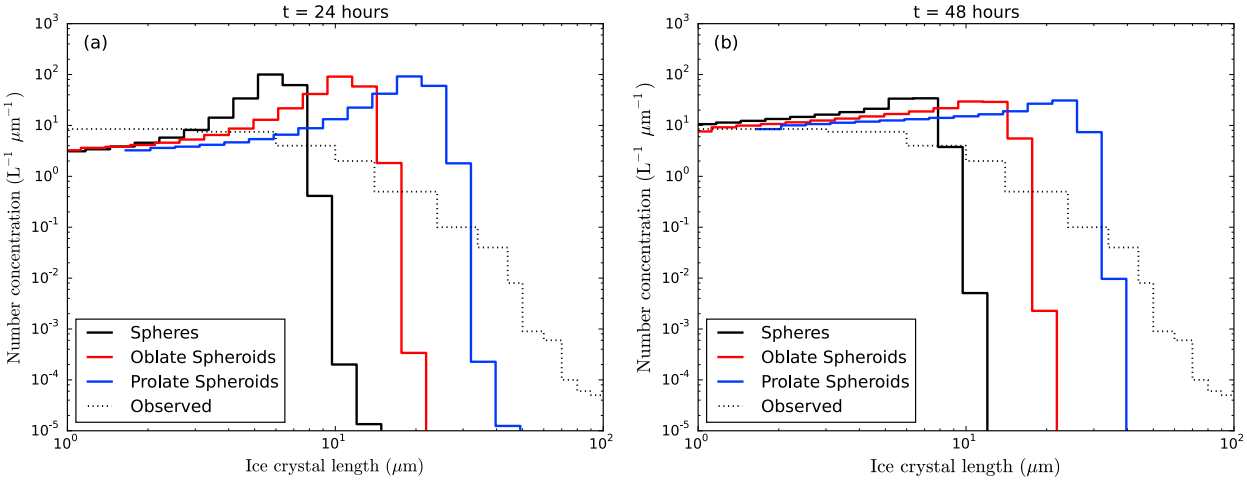

Figure 10. Ice crystal size distributions at (a) 24 hours and (b) 48 hours from runs with all spheres (Control), all oblate spheroids (Oblate-Full) and all prolate spheroids (Prolate-Full) with aspect ratios of 6. Observations taken from TTL cirrus over the Eastern Pacific [*Lawson et al.*, 2008].